Elucidation of synaptonemal complex organization by super-resolution imaging with isotropic resolution

Katharina Schücker[a,1], Thorge Holm[b,1], Christian Franke[b], Markus Sauer[b,2], and Ricardo Benavente[a,2]

Departments of [a]Cell and Developmental Biology and [b]Biotechnology and Biophysics, Biocenter, University of Würzburg, 97074 Würzburg, Germany

Edited* by Jennifer Lippincott-Schwartz, National Institutes of Health, Bethesda, MD, and approved December 19, 2014 (received for review August 2, 2014)

Synaptonemal complexes (SCs) are meiosis-specific multiprotein complexes that are essential for synapsis, recombination, and segregation of homologous chromosomes, but the molecular organization of SCs remains unclear. We used immunofluorescence labeling in combination with super-resolution imaging and average position determination to investigate the molecular architecture of SCs. Combination of 2D super-resolution images recorded from different areas of the helical ladder-like structure allowed us to reconstruct the 3D molecular organization of the mammalian SC with isotropic resolution. The central element is composed of two parallel cables at a distance of ∼100 nm, which are oriented perpendicular to two parallel cables of the lateral element arranged at a distance of ∼220 nm. The two parallel cable elements form twisted helical structures that are connected by transversal filaments by their N and C termini. A single-cell preparation generates sufficient localizations to compile a 3D model of the SC with nanometer precision.

super-resolution imaging | synaptonemal complex | *d*STORM | meiosis | average position determination

The synaptonemal complex (SC) is a well-preserved meiosis-specific protein complex among different species (1, 2). As revealed by transmission electron microscopy (TEM), when fully assembled, SCs are 200-nm-wide, ribbon-like structures that extend all along a chromosome bivalent (3, 4). SCs have a characteristic ladder-like organization that is highly conserved through evolution and consists of two lateral elements (LEs), at which chromatin of homologous chromosomes is attached, and a central region (CR). The CR holds the homologous chromosomes together and is made up of numerous transversal filaments (TFs) and the central element (CE).

At present, seven protein components of the synaptonemal complex have been identified in mammals, namely, the LE proteins SYCP2 and SYCP3 (5, 6); the TF protein SYCP1 (7); and the CE-specific proteins SYCE1, SYCE2, SYCE3, and TEX12 (8–10) (Figs. S1 and S2). However, in addition to the identification of SC protein components and the investigation of interaction partners, the establishment of a model of the molecular architecture remains indispensable for the understanding of its function and assembly process. Due to the resolution limit of conventional fluorescence microscopy, information about the molecular organization of SCs has been mainly obtained by immunogold EM (11). In standard immunogold EM preparations, gold particles are localized with nanometer resolution and the localization precision is mainly limited by the size of the primary and secondary IgG antibodies and the gold signal density (12–14). However, sample preparation is time-consuming and quantitative analysis of the signal is tedious because of the low binding efficiency of gold-labeled antibodies. Because the structural resolution is also determined by the labeling density (15), immunogold EM cannot visualize the different SC proteins as continuous structures. Therefore, the construction of localization maps of different proteins within the SC by immunogold EM remains challenging.

Recent advances in super-resolution imaging based on single-molecule localization (16, 17) provide spatial resolutions that are well below the diffraction limit, approaching virtually molecular resolution. In addition, fluorophore-labeled antibodies exhibit a higher binding affinity enabling the visualization of SC proteins as continuous structures. Hence, in combination with particle averaging methods, single-molecule localization microscopy can deliver localization maps of different proteins of multiprotein complexes with high precision (18, 19).

Because meiotic germ cells can be prepared for microscopic analysis and highly specific antibodies directed against the different components are available, the SC is predestinated for structure determination using single-molecule localization microscopy. In this work, we used one- and two-color single-molecule localization microscopy by *direct* stochastic optical reconstruction microscopy (*d*STORM) (20, 21) to elucidate the molecular organization of the helical SC structure with isotropic nanometer precision.

Results and Discussion

dSTORM Can Resolve Single Protein Strands of the SC with Nanometer Precision. As demonstrated in previous studies, SC substructures (LEs and CR) cannot be resolved as individual structures in confocal laser scanning microscopy images. Different SC proteins appear to colocalize on a single strand (Fig. 1 *A–D*). In clear contrast, LEs and the CR are easily resolved as separate strands using SYCP3- and SYCP1-specific antibodies and *d*STORM (Fig. 1 *E–L*). Notably, *d*STORM can resolve the different spatial positions of the N and C termini of the TF protein SYCP1 (Fig. 2 *M–P*). TFs are built up of SYCP1 homodimers, and previous experiments have indicated that the C-terminal ends of SYCP1 dimers localize in LEs, whereas the N termini of SYCP1 dimers interact in the CE (7, 15, 22, 23). Our data confirm that the N termini localize in the CE. Furthermore, the C termini localize to

Significance

Synaptonemal complexes (SCs) are meiosis-specific, 200-nm-wide, ladder-like structures that are essential for synapsis, recombination, and segregation of homologous chromosomes. Despite its importance for the spatial organization of individual components during meiosis, the molecular architecture of the SC is still unknown. We used super-resolution imaging by *direct* stochastic optical reconstruction microscopy (*d*STORM), which provides subdiffraction resolution for structural investigation of the SC. The helical ladder-like structure allowed us to reconstruct the 3D molecular organization of the mammalian SC from 2D "frontal" and "lateral" views with isotropic resolution. In combination with particle averaging, we managed to elucidate the molecular organization of the mammalian SC with nanometer precision and unraveled previously unknown details of its molecular architecture.

Author contributions: M.S. and R.B. designed research; K.S. and T.H. performed research; K.S., T.H., and C.F. analyzed data; and K.S., T.H., C.F., M.S., and R.B. wrote the paper.

The authors declare no conflict of interest.

*This Direct Submission article had a prearranged editor.

Freely available online through the PNAS open access option.

[1]K.S. and T.H. contributed equally to this work.

[2]To whom correspondence may be addressed. Email: m.sauer@uni-wuerzburg.de or benavente@biozentrum.uni-wuerzburg.de.

This article contains supporting information online at www.pnas.org/lookup/suppl/doi:10.1073/pnas.1414814112/-/DCSupplemental.

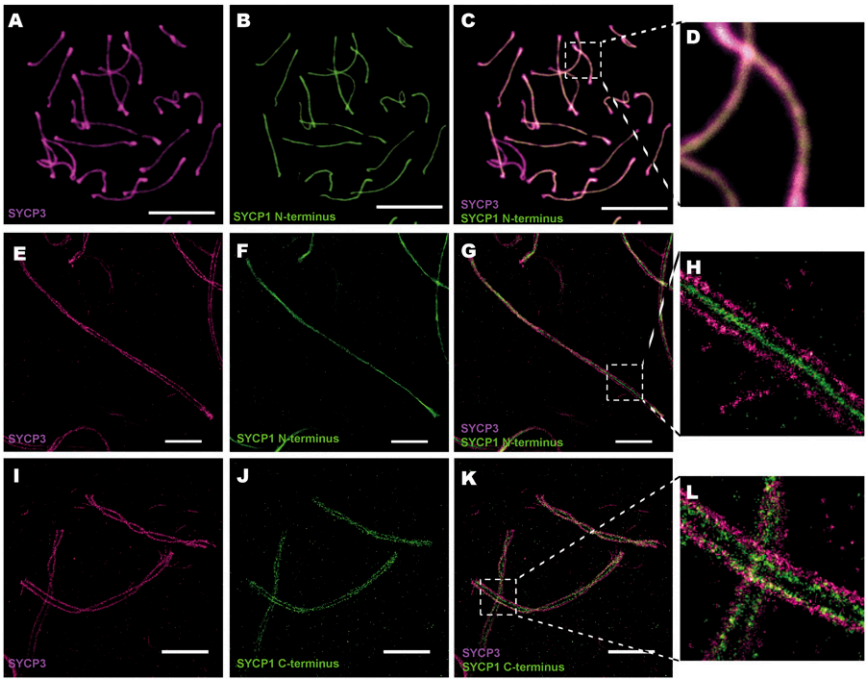

Fig. 1. Fluorescence imaging of SCs by standard and super-resolution imaging. Confocal laser scanning microscopy images (*A–D*) and *d*STORM images (*E–L*) are shown. (*A*) SYCP3 labeled with Texas Red. (*B*) SYCP1 N terminus labeled with Al488. (*C* and *D*) Overlay of *A* and *B* plus a magnified view. (*E*) SYCP3 labeled with Al647. (*F*) SYCP1 N terminus labeled with Al532. (*G* and *H*) Overlay of *E* and *F* plus a magnified view. (*I*) SYCP3 labeled with Al647. (*J*) SYCP1 C terminus labeled with Al532. (*K* and *L*) Overlay of *I* and *J* plus a magnified view. (Scale bars: *A–C*, 10 μm; *E–G* and *I–K*, 2 μm.)

the inner edge of the LEs (Fig. 1 *E–L*), indicating that the interaction of TFs with LE components takes place close to here and not deep in the LE. Consistent with immunogold EM and biochemical approaches, SYCP1 N termini overlap in the CE (15, 22, 23).

Our data also provide previously unidentified information about the molecular organization of proteins in the respective SC substructures. Regarding LEs, previous immunogold EM data suggested that SYCP2 is not homogeneously distributed in the LEs, as is the case for SYCP3, but enriched toward the inner edge of the LEs (22, 24). However, with the resolution provided by *d*STORM, the two proteins SYCP2 and SYCP3 appear to colocalize along the axial LE structures (Fig. 2 *A–D*).

To elucidate the molecular organization of the SC with nanometer precision and compile a molecular model, we determined the average positions of fluorescent probes with respect to the center of the helical structure (Fig. S3). To obtain 3D information about the spatial and axial localization of the different SC proteins, we did not use astigmatic (25) or biplane (26) imaging but took advantage of the fact that the SC shows a twisted helical structure. Imaging of the twisted and nontwisted areas allows the reconstruction of 3D protein maps from "frontal" and "lateral" 2D *d*STORM images, respectively, with isotropic resolution (Figs. 2 and 3). For quantitative analysis of the frontal and lateral distribution of SC proteins, one-color *d*STORM experiments were used exploiting the fact that the experimental conditions can be optimized for one fluorophore, Alexa Fluor 647 (Al647) in this case (20, 21). This approach allowed us to detect, on average, ~2,200 fluorescence photons per frame and single fluorescent probe, resulting in a localization precision of <10 nm.

Advanced 3D Model Emerges from *d*STORM Analysis. Advantageously, a single-cell preparation generates sufficient localizations to compile a 3D model of SC proteins with isotropic nanometer precision (Fig. 4 and Movie S1). The *d*STORM images of SC frontal views show a narrow monomodal signal distribution for the SYCP1 N termini with a width of 39.8 ± 1.1 nm (SD) (Fig. 4*A* and Fig. S4*J*), which is consistent with the notion that the SYCP1 N termini are localized to the very center of the CR (Figs. 1*H*, 2*P*, and 3 *D–F*). Available data suggest that SYCE3 binds directly to SYCP1, although the binding site is not known (10, 11). The SYCE3 signal distribution (Figs. 2 *H* and *L* and 3 *A–C*) is also monomodal, but wider [67.8 ± 2.1 nm (SD)] than the signal distribution of SYCP1 N termini (dotted lines of SYCP1 N termini and SYCE3 localizations in the frontal view are shown in Fig. 4*A* and Fig. S4*I*). This observation is in agreement with immunogold EM data (10) and might imply that SYCE3 binding to SYCP1 is not restricted to its N terminus. The signal distribution of SYCE2 [63.3 ± 2.1 nm (SD)] is slightly, but significantly, more narrow compared with SYCE3 and overlaps with the SYCP1 N terminus signal in agreement with previous coimmunoprecipitation experiments (9, 11) (Fig. 4 and Fig. S4*H*). The signal distribution of SYCE1 is 54.8 ± 2.8 nm (i.e., still narrower compared with SYCE2) (Fig. S4*G*). However, because the localization distributions clearly overlap, SYCE1 can interconnect with other CE proteins (Fig. 4).

The *d*STORM images of the twisted areas (lateral views) revealed bubbles (i.e., areas with bimodal distributions of SYCE1, SYCE2, SYCE3, and SYCP1 N termini) (Figs. 3 and 4*B* and Fig. S4). At these sites, the signals split into two parallel lines separated by a small interspace (Figs. 2*L*, 3, and 4*B*). The distribution of SYCP1 N termini and SYCE3, SYCE2, and SYCE1 localizations depicts two helical cables separated by 99.1 ± 4.8 nm (SD), 105.5 ± 5.3 nm (SD), 107.0 ± 4.6 nm (SD), and 96.7 ± 8.8 nm (SD), respectively, in lateral views (Fig. 4*B* and Fig. S4). The parallel cables of the CE are oriented perpendicular to the parallel cables of the LE. Here, it has to be pointed out that the degree of the dip in the bimodal distributions of these CE proteins can be affected by the size of the antibodies and the corresponding restricted accessibility of protein epitopes. The appearance of a bimodal distribution of all central proteins in lateral views independent of their relative positions (Fig. 4*B*) demonstrates the existence of at least two longitudinal cables in the CE composed of SYCP1,

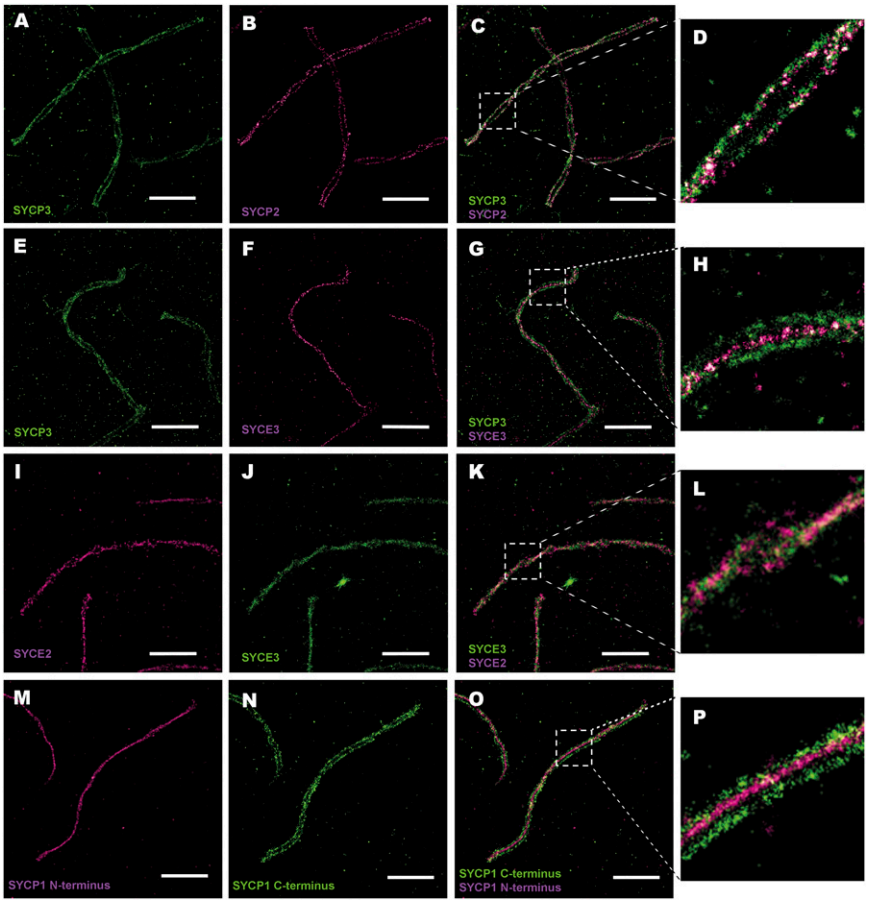

Fig. 2. Two-color *d*STORM images of the SC. (*A*) SYCP3 labeled with Al532. (*B*) SYCP2 labeled with Al647. (*C* and *D*) Overlay of *A* and *B* and a magnified view. (*E*) SYCP3 labeled with Al532. (*F*) SYCE3 labeled with Al647. (*G* and *H*) Overlay of *E* and *F* and a magnified view. (*I*) SYCE2 labeled with Al647. (*J*) SYCE3 labeled with Al532. (*K* and *L*) Overlay of *I* and *J* and a magnified view. (*M*) SYCP1 N terminus labeled with Al647. (*N*) SYCP1 C terminus labeled with Al532. (*O* and *P*) Overlay of *M* and *N* and a magnified view. (Scale bars: 2 μm.)

SYCE3, SYCE2, and SYCE1 that overlap axially in *d*STORM images taken from frontal views of the SC (Figs. 2 *I–L*, 3, and 4 and Fig. S4). In previous immunogold EM studies, no indication for a bimodal distribution of either of these proteins has ever been obtained. However, our results are in agreement with previous TEM data showing that TFs are organized in more than one layer (3, 4, 8–10, 15, 23, 27) (Fig. S2).

Both proteins of the LEs, SYCP3 and SYCP2, are arranged as two cables separated by 221.6 ± 6.1 nm (SD) and 218.5 ± 6.4 nm (SD), respectively (Figs. 2 *A–D* and 4*A*). SYCP3 and SYCP2, showing distribution widths of 55.8 ± 2.3 nm (SD) and 51.2 ± 1.2 nm (SD), respectively, colocalize on the LEs (Fig. 4*A* and Fig. S4 *B* and *D*). The helical LE structure surrounds the CR proteins SYCP1, SYCE3, SYCE2, and SYCE1, which are also arranged as two vertical twisted cables. Overall, the CR exhibits a width of 148.2 ± 2.6 nm (SD), as defined by the average positions of the two SYCP1 C-terminal signals (Fig. 4*A*). The C-terminal SYCP1 signal distribution shows a width of 45.2 ± 1.5 nm (SD) (Fig. 4*A*). With typical data sizes of five to seven SCs investigated per prepared cell nucleus, the SE of position determination is in the range of 0.6–2.4 nm.

Our study demonstrates that the SC represents ideal requirements for 3D molecular structure investigation by single-molecule localization microscopy (Fig. 4*C* and Movie S1). It shows a helical structure allowing position determination with isotropic resolution, it can easily be prepared on coverslips, its protein components can specifically be labeled by antibodies with low background, and a single preparation delivers enough data for model compilation with low statistical error. We predict that future single-molecule localization microscopy studies using selected combinations of antibodies will allow even deeper insights into the molecular organization of the SC and its interaction with other multiprotein complexes of the recombination machinery and the nuclear envelope.

Materials and Methods

Details on material and methods can be found in *SI Material and Methods*. Animal care was approved by the regulatory agency of the city of Würzburg (reference FB VVL 568/300-1870/13; according to §11/1 no. 1 of the German Animal Welfare Act, German Ministry of Agriculture, Health and Economics Cooperation).

Murine Spermatocyte Cell Spread Preparation. For cell spreading, we dissected testes from WT mice and followed the protocol described by de Boer et al. (28). For *d*STORM analysis, we used coverslips (24 × 60 mm) that we coated with 0.01% (wt/vol) poly-L-lysine for 5 min. We preferred coverslips instead of slides for SC spreading, because coverslips allow the use of total internal reflection fluorescence (TIRF) or highly inclined and laminated optical sheet (HILO) illumination schemes (29).

Photoswitching Buffer. For photoswitching, a 100 mM β-mercaptoethylamine buffer (MEA; Sigma) in PBS with a pH of 7.4–7.7 for one-color measurements (Al647) and a pH of 8.4–8.5 for two-color experiments (Al647 and Al532) was used. For recordings that were used for distance measurements, an oxygen scavenger system containing 10% (wt/vol) glucose and 0.5 mg/mL glucose oxidase was used.

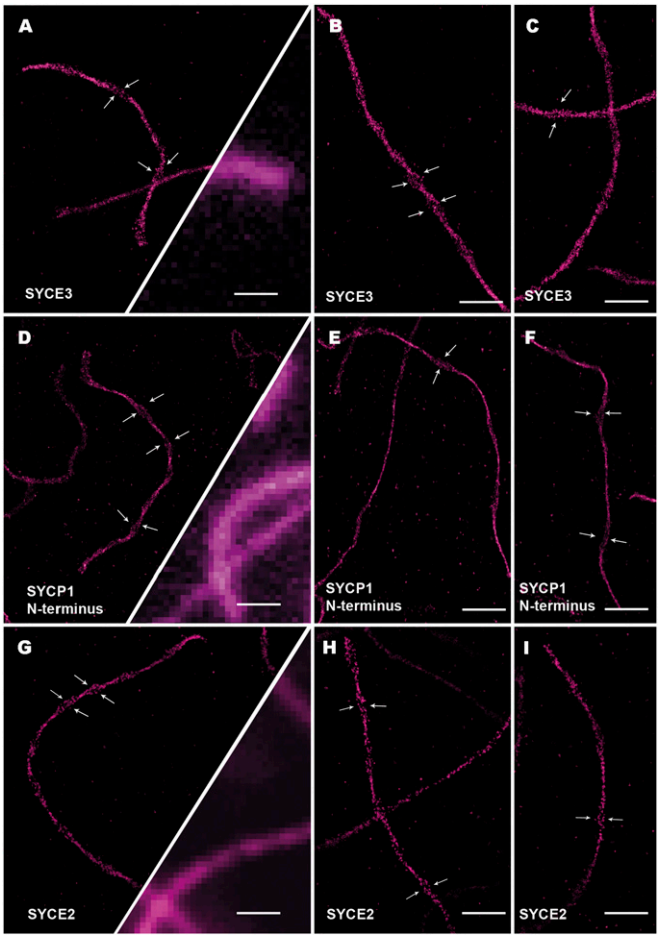

Fig. 3. Lateral view *d*STORM images of SYCE3, SYCP1, and SYCE2 reveal two parallel lines separated by ~100 nm. SYCE3 (*A–C*), the SYCP1 N terminus (*D–F*), and SYCE2 (*G–I*) were labeled with Al647. In *A* (*Lower Right*), *D* (*Lower Right*), and *G* (*Lower Right*), conventional TIRF wide-field fluorescence images are shown for resolution comparison. The arrows illustrate regions where the SC is twisted and seen from the side (lateral views). (Scale bars: 1 μm.)

Super-resolution Imaging. Super-resolution imaging by *d*STORM was performed using an inverted wide-field fluorescence microscope as described in more detail by van de Linde et al. (21). Briefly, for excitation of Al647 and Al532, a 639-nm OPSLaser-Diode System (Genesis MX639-1000 STM; Coherent) and a 514-nm OPSLaser-Diode System (Genesis MX514 STM; Coherent) were used. Al647 was always imaged before Al532 to minimize photobleaching. Lasers were spectrally cleaned by bandpass filters (FF01-642/10-25; Semrock or ZET 514/10; Chroma) and overlaid by a LaserMUX filter (LM01-552; Semrock). Laser beams were widened and focused onto the back focal plane of the microscope objective (APON 60XOTIRF; Olympus) by a lens system assembled with 25-mm (G322284000; Qioptiq) and 120-mm (G322303000; Qioptiq) focal length achromatic lens. The laser beam is directed into the back port of the inverse microscope (IX71; Olympus) by a broad-band dielectric mirror (KCB2 and BB2-E02; Thorlabs) and is reflected into the objective by a triple-band dichroic beam splitter (FF425/532/656-Di01; Semrock). The lens system and the dielectric mirror are mounted on a custom-made linear translation stage to switch between EPI (illumination and detection on one side), HILO, and TIRF illumination. To minimize sample drift, the objective and the sample are mounted onto the nosepiece stage (IX2-NPS; Olympus). The fluorescent light from the sample is collected by the same objective and is transmitted by the dichroic beam splitter and a triple-band detection filter (Em01-R442/514/647; Semrock). Images of the yellow Al532 and red Al647 dyes are separated and spectrally filtered by a dichroic beam splitter (630dcxr; Chroma) and dichroic bandpass filters (FF01-582/75 and FF01-697/75; Semrock) mounted to a dual-camera adaptor (TuCam; Andor) onto two EM CCD cameras (iXon Ultra 897; Andor).

Conventional wide-field fluorescence images were taken at low laser intensities to prevent photoswitching and at exposure times depending on fluorescence intensities between 10 and 1,000 ms. For *d*STORM imaging, data stacks consisting of 15,000–30,000 images were recorded with frame rates of 50–100 frames per second and 10- to 20-ms exposure times, respectively, at excitation intensities of 1–3 kW·cm^{-2}.

Image Reconstruction and Alignment of Two-Color Imaging. Images were reconstructed using rapid*d*STORM 3.2 (30, 31). The *d*STORM images are shown with a pixel size of 10 nm. For two-color imaging, Al647 was recorded first and both cameras were aligned using multifluorescent beads. The image generated by Al532 was transformed onto the image of Al647 using landmarks (bUnwapJ; Fiji) (32). Chromatic shift between the two images of the two cameras was corrected using cross-correlations/elastic transformations.

Postprocessing of *d*STORM Data for Average Protein Position Determination. To gain quantitative information on the diameter of single strands, as well as the distance of potential double strands, an in-house written python routine was exercised (Fig. S3). First, candidates for single complexes were separated by applying a canny edge filter to the superresolved picture. The vertices of the resulting mask were used to crop localization sets of these candidates out of the rapid*d*STORM output. Candidates consisting of crossing complexes or featuring extreme curvature, close to a full circle, proved inaccessible to further analysis. Using a mean component analysis of the *x* and *y* components of the localization set, those candidates were discarded, exhibiting a ratio of the absolute values of both eigenvectors smaller than 3. Next,

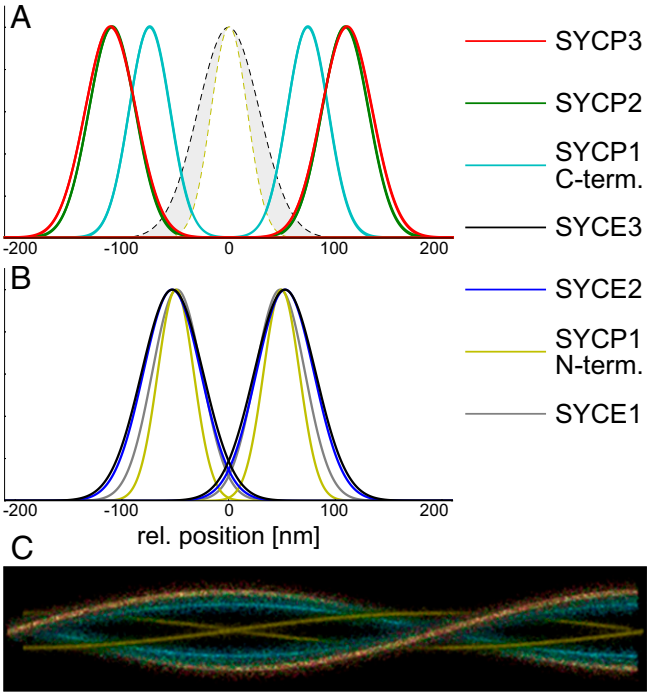

Fig. 4. Localization distributions and 3D reconstruction of the SC as revealed by *d*STORM and particle averaging. (*A*) Frontal view showing the bimodal distribution of the LE proteins SYCP2 and SYCP3 and the SYCP1 C terminus in continuous lines. The monomodal distributions of the CE protein SYCE3 and the SYCP1 N terminus are plotted in dotted lines. (*B*) Lateral view showing the bimodal distributions of CE proteins SYCE1, SYCE2, and SYCE3, as well as the SYCP1 N terminus. (*C*) Three-dimensional model of protein distributions of SYCP3 (red), SYCP2 (green), the SYCP1 C terminus (cyan), and the SYCP1 N terminus (yellow). Solid cables show averaged protein positions with the width of the SD of the averaged position (6.07 nm for SYCP3, 6.39 nm for SYCP2, 2.58 nm for the SYCP1 C terminus, and 4.84 nm for the SYCP1 N terminus). Cloudy dots indicate measured FWHM of single-molecule localization distributions (55.8 nm for SYCP3, 51.1 nm for SYCP2, 45.2 nm for the SYCP1 C terminus, and 39.8 nm for the SYCP1 N terminus).

a high-order ($n > 10$) polynomial was fitted to the data. Using this polynomial as a guideline, a sliding window algorithm was applied. The edge length parallel to the polynomial was thereby 50 nm, and the vertical edge length was chosen to be sufficiently larger than the expected double-strand distance (~1,000 μm). For each step, this window was moved 25 nm along the polynomial, providing a 25-nm overlap to the previous and next segments. For each segment, all distances between all inlying localizations were determined and histogrammed after projecting the distances perpendicular to the current slope of the polynomial. This histogram is then the basis for the calculation of strand diameter and double-strand distance. First, a fit of a bi-Gaussian distribution is attempted, and if successful, both peak values are stored. Thereby, the larger peak value stands for the mean distance of the two strands and the smaller peak value stands for the SD of localizations within the single strands in the current segment. If the bi-Gaussian fitting is unsuccessful, a mono-Gaussian model is applied to determine the spatial SD of the current segment, representing the diameter. To avoid falsifications due to unclean signals at the tail sections of the complexes, 100- to 500-nm segments from both sides of the complex were usually excluded from the final analysis. The left entirety of all diameter/distance values (originating from each segment) along the strand is then again histogrammed to determine the mean values for a single complex (via a bi- or mono-Gaussian fit of the final histogram). For each species, 30–50 complete complexes were processed, resulting in overall mean values of double-strand distance (if existing) as well as the FWHM of single strands (derived from the SD) for each protein (Fig. 4 *A* and *B* and Fig. S4). If not stated otherwise, all stated error margins are the SD of the individual protein statistic.

ACKNOWLEDGMENTS. We thank Howard Cooke (Medical Research Council Human Genetics Unit) for the provision of the antibody guinea pig anti-SYCE2 and rabbit anti-SYCE1. This work was supported by a grant of the Deutsche Forschungsgemeinschaft, Priority Program 1384–Mechanisms of Genome Haploidization (to R.B.). M.S. acknowledges the financial support of the Biophotonics Initiative of the Bundesministerium für Bildung und Forschung (Grants 13N11019 and 13N12507).

1. von Wettstein D, Rasmussen SW, Holm PB (1984) The synaptonemal complex in genetic segregation. *Annu Rev Genet* 18:331–413.
2. Zickler D, Kleckner N (1998) The leptotene-zygotene transition of meiosis. *Annu Rev Genet* 32:619–697.
3. Moses MJ (1968) Synaptinemal complex. *Annu Rev Genet* 2:363–412.
4. Wettstein R, Sotelo JR (1971) The molecular architecture of synaptonemal complexes. *Adv Mol Cell Biol* 1:109–152.
5. Lammers JH, et al. (1994) The gene encoding a major component of the lateral elements of synaptonemal complexes of the rat is related to X-linked lymphocyte-regulated genes. *Mol Cell Biol* 14(2):1137–1146.
6. Offenberg HH, et al. (1998) SCP2: A major protein component of the axial elements of synaptonemal complexes of the rat. *Nucleic Acids Res* 26(11):2572–2579.
7. Meuwissen RL, et al. (1992) A coiled-coil related protein specific for synapsed regions of meiotic prophase chromosomes. *EMBO J* 11(13):5091–5100.
8. Costa Y, et al. (2005) Two novel proteins recruited by synaptonemal complex protein 1 (SYCP1) are at the centre of meiosis. *J Cell Sci* 118(Pt 12):2755–2762.
9. Hamer G, et al. (2006) Characterization of a novel meiosis-specific protein within the central element of the synaptonemal complex. *J Cell Sci* 119(Pt 19):4025–4032.
10. Schramm S, et al. (2011) A novel mouse synaptonemal complex protein is essential for loading of central element proteins, recombination, and fertility. *PLoS Genet* 7(5): e1002088.
11. Fraune J, Schramm S, Alsheimer M, Benavente R (2012) The mammalian synaptonemal complex: Protein components, assembly and role in meiotic recombination. *Exp Cell Res* 318(12):1340–1346.
12. Weber K, Rathke PC, Osborn M (1978) Cytoplasmic microtubular images in glutaraldehyde-fixed tissue culture cells by electron microscopy and by immunofluorescence microscopy. *Proc Natl Acad Sci USA* 75(4):1820–1824.
13. Baschong W, Wrigley NG (1990) Small colloidal gold conjugated to Fab fragments or to immunoglobulin G as high-resolution labels for electron microscopy: A technical overview. *J Electron Microsc Tech* 14(4):313–323.
14. Schmekel K, et al. (1996) Organization of SCP1 protein molecules within synaptonemal complexes of the rat. *Exp Cell Res* 226(1):20–30.
15. Shannon CE (1949) Communication in the presence of noise. *Proc IEEE Inst Electr Electron Eng* 37:10–21.
16. Patterson G, Davidson M, Manley S, Lippincott-Schwartz J (2010) Superresolution imaging using single-molecule localization. *Annu Rev Phys Chem* 61:345–367.
17. Sauer M (2013) Localization microscopy coming of age: From concepts to biological impact. *J Cell Sci* 126(Pt 16):3505–3513.
18. Löschberger A, et al. (2012) Super-resolution imaging visualizes the eightfold symmetry of gp210 proteins around the nuclear pore complex and resolves the central channel with nanometer resolution. *J Cell Sci* 125(Pt 3):570–575.
19. Szymborska A, et al. (2013) Nuclear pore scaffold structure analyzed by super-resolution microscopy and particle averaging. *Science* 341(6146):655–658.
20. Heilemann M, et al. (2008) Subdiffraction-resolution fluorescence imaging with conventional fluorescent probes. *Angew Chem Int Ed Engl* 47(33):6172–6176.
21. van de Linde S, et al. (2011) Direct stochastic optical reconstruction microscopy with standard fluorescent probes. *Nat Protoc* 6(7):991–1009.
22. Winkel K, Alsheimer M, Öllinger R, Benavente R (2009) Protein SYCP2 provides a link between transverse filaments and lateral elements of mammalian synaptonemal complexes. *Chromosoma* 118(2):259–267.
23. Liu JG, et al. (1996) Localization of the N-terminus of SCP1 to the central element of the synaptonemal complex and evidence for direct interactions between the N-termini of SCP1 molecules organized head-to-head. *Exp Cell Res* 226(1):11–19.
24. Tarsounas M, Pearlman RE, Gasser PJ, Park MS, Moens PB (1997) Protein-protein interactions in the synaptonemal complex. *Mol Biol Cell* 8(8):1405–1414.
25. Huang B, Wang W, Bates M, Zhuang X (2008) Three-dimensional super-resolution imaging by stochastic optical reconstruction microscopy. *Science* 319(5864):810–813.
26. Juette MF, et al. (2008) Three-dimensional sub-100 nm resolution fluorescence microscopy of thick samples. *Nat Methods* 5(6):527–529.
27. Öllinger R, Alsheimer M, Benavente R (2005) Mammalian protein SCP1 forms synaptonemal complex-like structures in the absence of meiotic chromosomes. *Mol Biol Cell* 16(1):212–217.
28. de Boer E, Lhuissier FG, Heyting C (2009) Cytological analysis of interference in mouse meiosis. *Methods Mol Biol* 558:355–382.
29. Tokunaga M, Imamoto N, Sakata-Sogawa K (2008) Highly inclined thin illumination enables clear single-molecule imaging in cells. *Nat Methods* 5(2):159–161.
30. Wolter S, et al. (2010) Real-time computation of subdiffraction-resolution fluorescence images. *J Microsc* 237(1):12–22.
31. Wolter S, et al. (2012) rapidSTORM: Accurate, fast open-source software for localization microscopy. *Nat Methods* 9(11):1040–1041.
32. Arganda-Carreras I, et al. (2006) Consistent and elastic registration of histological sections using vector-spline regularization. *Lecture Notes in Computer Science* 4241: 85–95.